Polymer Chemistry

ROYAL SOCIETY OF CHEMISTRY

PAPER

View Article Online
View Journal | View Issue

Check for updates

Cite this: *Polym. Chem.*, 2024, **15**, 4005

Emissive covalent organic frameworks with abundant interaction sites for hydrazine sensing†

Yuwei Zhang, [a] Ce Xing,[a] Zhibin Tian,[b] Wanyi Zhao,[a] Yongfeng Zhi,*[b] Lina Zhao*[a] and He Li *[c]

Received 24th July 2024,
Accepted 15th September 2024

DOI: 10.1039/d4py00815d

rsc.li/polymers

Covalent organic frameworks (COFs) possess versatile advantages, including their lightweight nature, exceptional stability, and having a well-defined π structure, rending them highly promising for fluorescence sensors. One of the most important factors for sensing is the presence of interaction sites, which previous research has not considered extensively. In this study, we present the synthesis of two emissive hydrazone-linked COFs (EH-COFs) under solvothermal conditions. The hydrazone linkages, which contain –NH single bond groups on the walls, reduce aggregation-caused fluorescence quenching, resulting in enhanced emission activity. Furthermore, the abundance of interaction sites (nitrogen and oxygen atoms) on the walls enables efficient interaction with guest molecules. Owing to these advantages, EH-COFs exhibited elevated sensitivity and selectivity, with low detection limits, for hydrazine sensing, ranking them among the top-performing fluorescence probes reported to date.

Introduction

Hydrazine is a flammable and explosive molecule commonly utilized as a propellant in missile and rocket propulsion systems. Additionally, owing to its reducing properties and alkalinity, hydrazine serves as a precursor for polymer and drug synthesis.[1–3] However, it poses significant hazards to human health, such as teratogenic and carcinogenic effects, particularly when present in high concentrations in the environment. Therefore, there is an urgent need to develop a sensitive and efficient method for detecting hydrazine in living environments. Traditionally, hydrazine detection has relied on spectrophotometry, chemical titration, and electrochemical methods, which are known for their complexity, time-consuming nature, and high cost. However, recent advancements in luminescence sensors have provided a simpler, more sensitive, and cost-effective solution for hydrazine detection. These sensors utilize various materials, including small molecules, polymers, and composites as probes, and detect changes in luminescence to detect hydrazine.[4–7]

Compared with traditional fluorescent probes, covalent organic frameworks (COFs) have garnered significant attention due to their distinctive characteristics.[8–13] COFs represent a novel class of porous organic materials renowned for their exceptional crystalline structure and uniform nano-pore architecture.[14–16] These inherent advantages have propelled COFs to the forefront of materials research, attracting considerable interest across diverse applications such as substance adsorption, catalysis, and energy devices.[17–38]

COFs have exhibited significant advancements as fluorescent chemical sensors. In contrast to conventional chemical sensors, COFs possess a permanent pore structure, which offers abundant space for the capturing of guest molecules.[8,9] Moreover, the precise pore structure and active sites in the channel facilitate targeted interactions with complex analytes.[10–14] Additionally, COFs featuring π-linked structures contribute to signal amplification, which is a critical factor in trace target detection.[9,29–31] Given these advantages, COFs exhibit high specificity and sensitivity, garnering widespread acclaim.[32–36] Numerous studies have emphasized the effectiveness of luminescent COFs in detecting hazardous explosive molecules, metal ions, anions, and pH levels.[37–49] However, conventional COFs often lack adequate detection sites, which may lead to overlooking certain analytes.

In this study, we synthesized two emissive hydrazone-linked COFs (EH-COFs, chemical structure as shown in Fig. 1) under solvothermal conditions. The design of EH-COFs was guided by several considerations. Firstly, we introduced hydrazone linkages with –NH groups on the walls, characterized by single bonds, which weaken aggregation-caused fluorescence

[a]*Laboratory of Preparation and Applications of Environmental Friendly Materials (Jilin Normal University), Ministry of Education, Changchun, 130103, China. E-mail: zhaolina1975@163.com*
[b]*School of Chemistry and Chemical Engineering, Hainan University, Haikou, 570228, China. E-mail: zhiyf@hainanu.edu.cn*
[c]*Division of Energy Materials, Dalian Institute of Chemical Physics, Chinese Academy of Sciences, Dalian 116023, China. E-mail: lihe@dicp.ac.cn*
† Electronic supplementary information (ESI) available. See DOI: https://doi.org/10.1039/d4py00815d

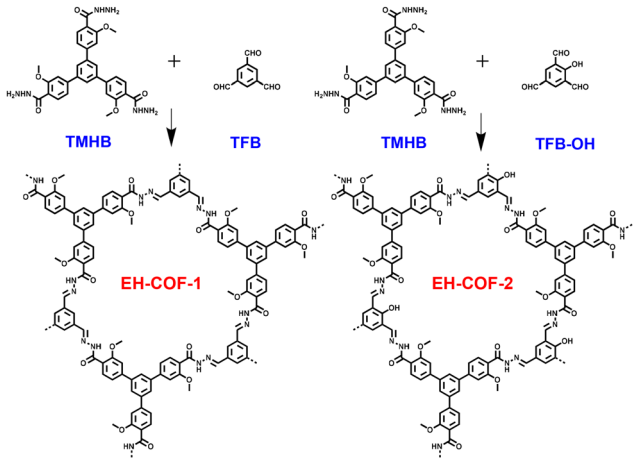

Fig. 1 Design and synthesis of EH-COFs.

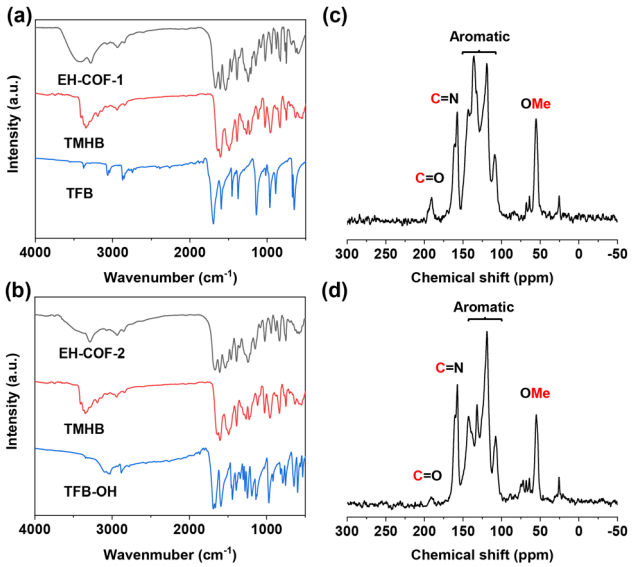

Fig. 2 (a and b) FT-IR spectra of EH-COFs and building units. ^{13}C NMR spectra of (c) EH-COF-1 and (d) EH-COF-2.

quenching.[38–42] Additionally, the incorporation of –OH groups adjacent to the Schiff-base centers facilitates intramolecular hydrogen bonding, enhancing the chemical stability of EH-COF-2.[43–46] Furthermore, the abundance of nitrogen atoms and oxygen on the walls allows for interaction with guest molecules. Consequently, EH-COFs have emerged as attractive candidates for the development of novel molecular sensors. As anticipated, the EH-COFs exhibited strong crystallinity, excellent stability, high luminescence efficiency, and abundant active sites. Most notably, EH-COFs demonstrated high sensitivity and selectivity as a fluorescent probe for hydrazine sensing, attributable to their synergistic structural features.

Results and discussion

EH-COFs were synthesized by heating a suspension of 1,3,5-tris(3′-methoxy-4′-hydrazinecarbonylphenyl)benzene (TMHB) and 1,3,5-triformyl benzene (TFB) or 2-hydroxybenzene-1,3,5-tricarbaldehyde (TFB-OH) in the presence of aqueous acetic acid as catalyst (Fig. 1). The structure of the building units was confirmed through proton NMR spectroscopy, as detailed in Schemes S1–S3.† The Fourier transform infrared spectroscopy (FT-IR) spectra of EH-COFs and the monomers was investigated to confirm the successful synthesis. The FT-IR spectrum of EH-COF-1 exhibited a stretching vibration band at 1617 cm^{-1}, which was attributed to the C=N bond (Fig. 2a, black). Notably, there was no stretching vibration band corresponding to the aldehyde group at 1697 cm^{-1} from TFB (Fig. 2a, blue), indicating the complete condensation of the monomers. Similarly, EH-COF-2 showed the C=N bond vibration at 1609 cm^{-1} (Fig. 2b, black), with no remaining aldehyde structure (Fig. 2b, blue). Additionally, the –OMe group information was observed around 2800–3000 cm^{-1}, confirming the presence of methoxy groups. These results suggest the successful synthesis and structural integrity of the EH-COFs. Solid-state ^{13}C nuclear magnetic resonance (^{13}C NMR) of EH-COF-1 and EH-COF-2 exhibited the carbon signals of imine linkage at 158 and 157 ppm, respectively (Fig. 2c and d). In addition, the carbon of –OMe units is located at 56 and 55 ppm for EH-COF-1 and EH-COF-2, respectively. The carbon of aromatic rings is observed from 108 to 146 ppm for EH-COFs. Field emission scanning electron microscope images of EH-COFs were investigated to reveal their uniform stacking morphology. EH-COFs exhibited a uniform belt-like structure (Fig. S1†). Energy dispersive X-ray spectroscopy (EDS) mapping images showed the uniform distribution of C, N, and O elements (Fig. S2 and S3†).

We examined the porous properties of the EH-COFs using nitrogen adsorption–desorption measurements. According to the IUPAC classification, EH-COFs exhibited a combination of type-I and type-IV nitrogen sorption isotherm features (Fig. S4a and S5a†). The microporous nature was evident in the P/P_0 range of 0 to 0.1, attributable to the steep increase in nitrogen uptake within this range. The Brunauer–Emmett–Teller (BET) specific surface area of EH-COF-1 and EH-COF-2 was found to be 316 and 187 m^2 g^{-1}, respectively. Both EH-COFs exhibit microporous characteristics, with pore diameters mainly distributed at 1.8 nm (Fig. S4b and S5b†).

The powder X-ray diffraction (PXRD) analysis results indicated their highly crystalline structure. EH-COF-1 exhibited PXRD peaks at 4.60°, 8.04°, 9.42°, 12.42°, and 25.86°, assigned to the (100), (110), (200), (210), and (001) facets, respectively (Fig. 3a, red). EH-COF-2 displayed PXRD peaks at 4.64°, 8.22°, 9.33°, 12.34°, and 26.05°, corresponding to the (100), (110), (200), (210), and (001) facets, respectively (Fig. 3b, red). After Pawley refinement of unit cells, the AA stacking model for EH-COFs aligned with experimental results, while the AB model failed to match. The unit crystal structures of both COFs with AA stacking model are depicted in Fig. 3c and d (a = b = 21.7401 Å, c = 3.7230 Å, α = β = 90.00°, γ = 120.00° for

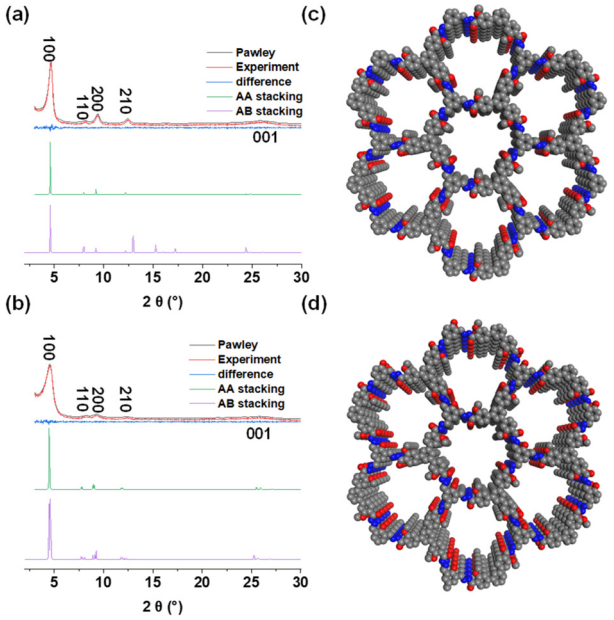

Fig. 3 PXRD patterns of (a) EH-COF-1 and (b) EH-COF-2. Top views of the AA stacking structure for (c) EH-COF-1 and (d) EH-COF-2.

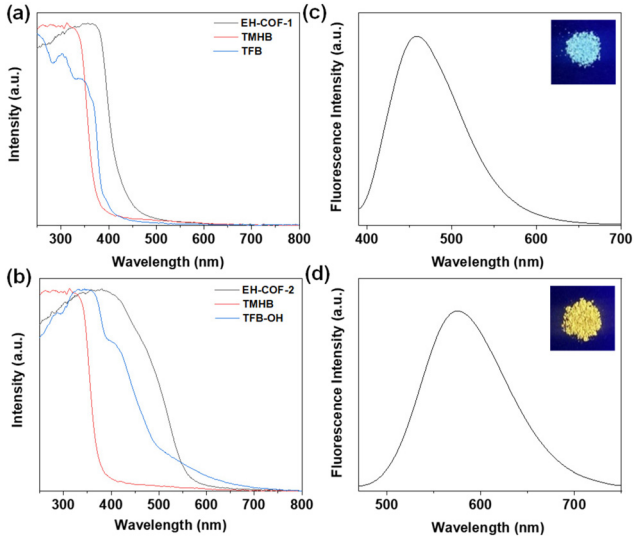

Fig. 4 Solid spectra of (a and b) EH-COFs and building units in the solid state. Fluorescence spectra of (c) EH-COF-1 and (d) EH-COF-2 in the solid state (inside their images under 365 nm).

EH-COF-1; a = 22.9190 Å, b = 22.5673 Å, c = 3.5273 Å, $\alpha = \beta$ = 90.43°, γ = 122.13° for EH-COF-2).

The stability of COFs is a crucial factor in their functional exploration. We assessed the chemical stability of EH-COF samples by exposing them into various solvents, including water, *N*,*N*-dimethylformamide, ethanol, 1 M HCl, and 1 M NaOH, for 24 hours at room temperature. Remarkably, EH-COF-1 and EH-COF-2 samples maintained strong PXRD patterns at their original positions after treatment, indicating that the excellent crystallinity of these two COFs is well-preserved under harsh conditions (Fig. S6†). Additionally, the FT-IR spectra of the COFs after treatment showed consistent vibration information across all samples (Fig. S7†). These results suggest that EH-COFs exhibit good chemical stability, which is essential for their functionalization and practical application. The ability to retain crystallinity and structural integrity under various chemical conditions underscores the robustness of EH-COFs, making them suitable for diverse environments and enhancing their potential applications.

The EH-COF-1 powder exhibited an electronic absorption band around 375 nm (Fig. 4a, black), which showed a red-shift compared to its building units. Similar results were found for EH-COF-2 with an absorption band at 390 nm (Fig. 4b, black). Additionally, the EH-COF-2 exhibited a highly conjugated skeleton owing to the presence of hydroxyl groups and nitrogen atoms, which resulted in hydrogen-bonding interactions. The EH-COF-1 displayed blue emission at 460 nm (Fig. 4c) when excited at 383 nm (Fig. S8a†) in the solid state. In contrast, the EH-COF-2 exhibited yellow fluorescence with an emission peak at 590 nm (Fig. 4d) when excited at 392 nm (Fig. S8b†).

EH-COF-1 and EH-COF-2 samples were dispersed in Phosphate Buffer Saline (PBS) buffer, which was applied to detect hydrazine (N_2H_4, 20 mM, pH = 7.4). In addition, EH-COFs kept stable in PBS buffer solutions under different conditions confirmed *via* the FT-IR and PXRD analysis in Fig. S9.† Fig. 5a and b show the fluorescence emission spectra of EH-COFs sample suspensions after adding different concentrations of hydrazine solution (0–10 μM). Surprisingly, when hydrazine was mixed with the EH-COFs in PBS buffer suspension, the fluorescence intensity of the original material was significantly quenched. For example, the fluorescence quenching degrees of EH-COF-1 and EH-COF-2 decreased by 73% and 67%, respectively. A good linear relationship was observed between the fluorescence intensity of EH-COFs and lower hydrazine concentration in Fig. 5c and d. The detection limit was estimated from the lower hydrazine concentration, which was down to 51 nM and 28 nM for EH-COFs, respectively, ranking as the best performance among reported COFs and metal–organic frameworks (Table S1†).[50–55] Additionally, the fluorescence quenching efficiency of the EH-COFs sensor can be nearly fitted to the Stern–Volmer equation, $I_0/I = K_{sv} \times [Q] + 1$, which relates the fluorescence intensity, where I_0 and I are the fluorescence intensities in the absence and presence of a quencher, respectively. [Q] represents the hydrazine concentration and K_{sv} is the quenching constant. According to the fluorescence titration of EH-COFs with hydrazine, a near curvier Stern–Volmer plot was obtained with a K_{sv} value of 2.3 × 10^5 M^{-1} (Fig. S10†). The results indicate an excellent sensitivity towards hydrazine detection owing to the active sites on the walls of EH-COFs.

To gain a deeper understanding of the quenching mechanism, we investigated the fluorescence lifetime of EH-COF with and without hydrazine (Fig. 5e and f). The fluorescence lifetime of EH-COF-1, which was initially 1.4 ns, was reduced to 1.3 ns in the presence of hydrazine. Similarly, the fluo-

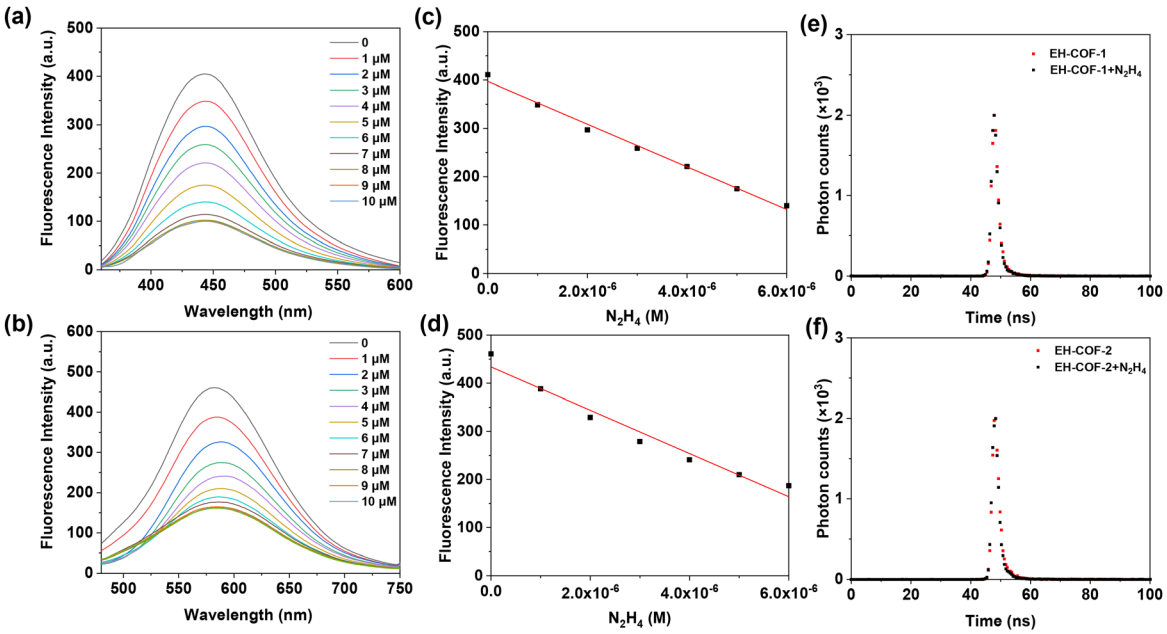

Fig. 5 Fluorescence spectra of (a) EH-COF-1 and (b) EH-COF-2 with different concentration of hydrazine. Fluorescence intensity of (c) EH-COF-1 and (d) EH-COF-2 with different concentration of hydrazine. Lifetimes of (e) EH-COF-1 and (f) EH-COF-2 with and without hydrazine.

rescence lifetime changed from 1.5 to 1.3 ns of EH-COF-2 with the addition of hydrazine. These results suggest that a photo-induced electron transfer (PET) process is responsible for the fluorescence quenching of EH-COFs.

Selectivity is crucial for sensors. To evaluate the sensing performance of EH-COFs under different acidic and alkaline conditions, we investigated the effect of pH on the fluorescence intensity of EH-COFs. As illustrated in Fig. 6a and b, within the pH range of 4 to 10, the fluorescence intensity of EH-COFs remained almost unchanged, indicating excellent pH stability. Upon the addition of hydrazine, the fluorescence intensity of the EH-COFs exhibited only slight fluctuations within this pH range, with a minimal decrease observed under strong acidic and alkaline conditions. This suggests that EH-COFs demonstrate robust stability and can be effectively utilized for hydrazine detection across a wide range of acidic and alkaline environments.

We further considered the potential interference from metal ions and anions. To explore the anti-interference and specific recognition properties of EH-COFs for hydrazine sensing, we selected common metal cations and anions as interference components. After adding these various interference components (as depicted by the orange bars in Fig. 6c, d and Fig. S9, S10†), the fluorescence emission intensity of EH-COFs remained almost unchanged, indicating minimal response to these common interference components. However, upon the addition of hydrazine (depicted by the green bars in Fig. 6c and d), there was a significant decrease in fluorescence intensity. This demonstrates the high sensitivity and specific recognition capability of EH-COFs for hydrazine detection. These results suggest that EH-COFs exhibit excellent selectivity for detecting hydrazine, maintain stability across a wide pH range and demonstrate minimal interference from common metal ions and anions.

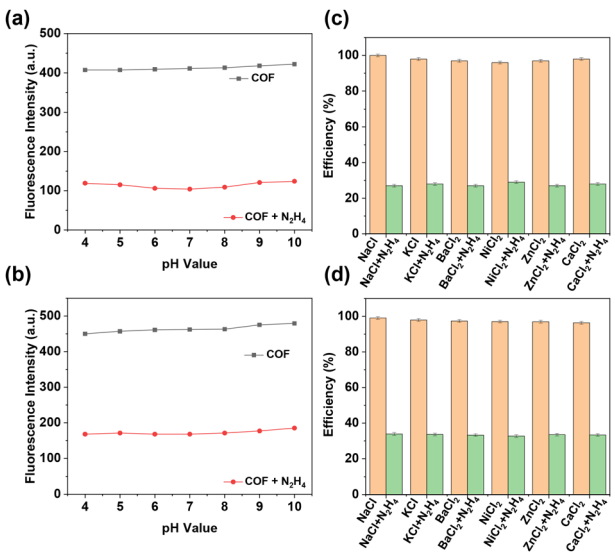

Fig. 6 Quenching efficiency of (a) EH-COF-1 and (b) EH-COF-2 under different pH values. Quenching efficiency of (c) EH-COF-1 and (d) EH-COF-2 with hydrazine and different ions.

Conclusions

In this study, we synthesized two emissive hydrazone-linked COFs known for their exceptional crystallinity, robust stability, and high luminescence efficiency. EH-COFs possess numerous

active sites on their walls, which significantly enhances the sensitivity and selectivity for hydrazine detection, surpassing existing benchmarks. The interaction between hydrazine and these active sites suggests a mechanism involving photo-induced electron transfer, leading to the quenching of fluorescence. These insights highlight the potential of leveraging multiple active sites to develop highly efficient fluorescence sensors with wide-ranging applications across various fields. The distinctive properties of EH-COFs position them as promising candidates for advancing sensor technologies. Their capability to address diverse analytical challenges and their potential to contribute to innovations in environmental monitoring and industrial processes underscore their significance. Future research could further explore the optimization of emissive COFs for specific sensing applications, potentially opening new avenues for advanced materials in the realm of sensor development.

Author contributions

Y. Zhang, C. Xing, Z. Tian, W. Zhao and Y. Zhi conducted experiments and collected data collection. Y. Zhi, L. Zhao and H. Li wrote the manuscript and discussed the results with all authors.

Data availability

The data supporting this article have been included as part of the ESI.†

Conflicts of interest

There are no conflicts to declare.

Acknowledgements

This work was financially supported by the National Natural Science Foundation of Jilin province (No. YDZJ202201ZYTS344), Hainan Provincial Nature Science Foundation of China (224QN181) and the National Key R&D Program of China (2021YFA1200401).

References

1 Z. Lu, W. Fan, X. Shi, Y. Lu and C. Fan, *Anal. Chem.*, 2017, **89**, 9918–9925.
2 J. Li, Y. Cui, C. Bi, S. Feng, F. Yu, E. Yuan, S. Xu, Z. Hu, Q. Sun, D. Wei and J. Yoon, *Anal. Chem.*, 2019, **91**, 7360–7365.
3 N. Vijay and S. Velmathi, *ACS Sustainable Chem. Eng.*, 2020, **8**, 4457–4463.
4 A. D. Arulraj, M. Vijayan and V. S. Vasantha, *Spectrochim. Acta, Part A*, 2015, **148**, 355–361.
5 Z. K. He, B. Fuhrmann and U. Spohn, *Anal. Chim. Acta*, 2000, **407**, 203–212.
6 Y. Y. Tang, C. L. Kao and P. Y. Chen, *Anal. Chim. Acta*, 2012, **711**, 32–39.
7 K. Zhang, Y. Huang, Y. J. Shen, S. Ma and T. T. Chen, *Talanta*, 2021, **225**, 122065.
8 X. Liu, D. Huang, C. Lai, G. Zeng, L. Qin, H. Wang, H. Yi, B. Li, S. Liu, M. Zhang, R. Deng, Y. Fu, L. Li, W. Xue and S. Chen, *Chem. Soc. Rev.*, 2019, **48**, 5266–5302.
9 L. Guo, L. Yang, M. Li, L. Kuang, Y. Song and L. Wang, *Coord. Chem. Rev.*, 2021, **440**, 213957.
10 P. J. Waller, F. Gándara and O. M. Yaghi, *Acc. Chem. Res.*, 2015, **48**, 3053–3063.
11 S. S. Zhu, Z. Zhang, Z. Li, H. Yue and X. Liu, *Chem Catal.*, 2024, **4**, 100963.
12 P. She, Y. Qin, X. Wang and Q. Zhang, *Adv. Mater.*, 2021, **34**, 2101175.
13 T. Zhang, G. Zhang and L. Chen, *Acc. Chem. Res.*, 2022, **55**, 795–808.
14 Z. Meng and K. A. Mirica, *Chem. Soc. Rev.*, 2021, **50**, 13498–13558.
15 D. Wei, W. Zhao, C. Xing, Y. Zhang, H. Li and Y. Zhi, *ACS Appl. Polym. Mater.*, 2024, **6**, 8498–8504.
16 Y. Feng, G. Wang, R. Liu, X. Ye, S. Tao, M. A. Addicoat, Z. Li, Q. Jiang and D. Jiang, *Angew. Chem., Int. Ed.*, 2024, **63**, e202400009.
17 Y. Shi, J. Yang, F. Gao and Q. Zhang, *ACS Nano*, 2023, **17**, 1879–1905.
18 J. Sun, Y. Xu, Y. Lv, Q. Zhang and X. Zhou, *CCS Chem.*, 2023, **5**, 1259–1276.
19 S. Xu and Q. Zhang, *Mater. Today Energy*, 2021, **20**, 100635.
20 D. Tan, R. Zhuang, R. Chen, M. Ban, W. Feng, F. Xu, X. Chen and Q. Wang, *Adv. Funct. Mater.*, 2024, **34**, 2311655.
21 C. Yang, Z. Zhang, J. Li, Y. Hou, Q. Zhang, Z. Li, H. Yue and X. Liu, *Green Chem.*, 2024, **26**, 2605–2612.
22 Y. Yusran, J. Xing, Q. Lin, G. Wu, W. Peng, Y. Wu, T. Su, L. Yang, L. Zhang, Q. Li, H. Wang, Z. Li and D. Zhang, *Small*, 2023, **19**, 2303069.
23 P.-K. Zhou, Y. Li, T. Zeng, M. Y. Chee, Y. Huang, Z. Yu, H. Yu, H. Yu, W. Huang and X. Chen, *Angew. Chem., Int. Ed.*, 2024, **63**, e202402911.
24 P.-K. Zhou, H. Yu, Y. Li, H. Yu, Q. Chen and X. Chen, *J. Polym. Sci.*, 2024, **62**, 1536–1553.
25 X. Wang, H. Liu, J. Zhang and S. Chen, *Polym. Chem.*, 2023, **14**, 1293–1317.
26 Z. Li, H. Moon, S. Cho, C. Li, J. Seo, J. Baek, H. Xu and S. Lee, *CCS Chem.*, 2023, **5**, 2567–2575.
27 Z. Li, L. Sun, L. Zhai, K.-S. Oh, J.-M. Seo, C. Li, D. Han, J.-B. Baek and S.-Y. Lee, *Angew. Chem., Int. Ed.*, 2023, **62**, e202307459.
28 C. Wang, W. Li, Y. Jin, J. Liu, H. Wang and Q. Zhang, *Small*, 2023, **19**, 2300023.
29 J. Ma, T. Shu, Y. Sun, X. Zhou, C. Ren, L. Su and X. Zhang, *Small*, 2021, **18**, 2103516.
30 T. Skorjanc, D. Shetty and M. Valant, *ACS Sens.*, 2021, **6**, 1461–1481.

31 G. Das, B. Garai, T. Prakasam, F. Benyettou, S. Varghese, S. K. Sharma, F. Gándara, R. Pasricha, M. Baias, R. Jagannathan, N. Saleh, M. Elhabiri, M. A. Olson and A. Trabolsi, *Nat. Commun.*, 2022, **13**, 3904.
32 Y. Liu, J. Ren, Y. Wang, X. Zhu, X. Guan, Z. Wang, Y. Zhou, L. Zhu, S. Qiu, S. Xiao and Q. Fang, *CCS Chem.*, 2023, **5**, 2033–2045.
33 D. Zhen, C. Liu, Q. Deng, S. Zhang, N. Yuan, L. Li and Y. Liu, *Chin. Chem. Lett.*, 2023, **35**, 109249.
34 S. Jiang, L. Meng, W. Ma, G. Pan, W. Zhang, Y. Zou, L. Liu, B. Xu and W. Tian, *Mater. Chem. Front.*, 2021, **5**, 4193–4201.
35 P. Das, G. Chakraborty, S. Tyagi and S. K. Mandal, *ACS Appl. Mater. Interfaces*, 2020, **12**, 52527–52537.
36 J. Zeng, X. Wang and X. Zhang, *Chem. – Eur. J.*, 2020, **26**, 16568–16581.
37 M. Yuan, F. Ma, X. Dai, L. Chen, F. Zhai, L. He, M. Zhang, J. Chen, J. Shu, X. Wang, X. Wang, Y. Zhang, X. Fu, Z. Li, C. Guo, L. Chen, Z. Chai and S. Wang, *Angew. Chem., Int. Ed.*, 2021, **60**, 21250–21255.
38 H. Qian, C. Dai, C. Yang and X. Yan, *ACS Appl. Mater. Interfaces*, 2017, **9**, 24999–25005.
39 Z. Li, K. Geng, T. He, K. T. Tan, N. Huang, Q. Jiang, Y. Nagao and D. Jiang, *Angew. Chem., Int. Ed.*, 2021, **60**, 19419–19427.
40 J. Feng, C. Hu, Y. Bai, Q. Su, S. Liu, M. Li, W. Wang, H. Ren and Q. Wu, *Microporous Mesoporous Mater.*, 2024, **366**, 112971.
41 Y. Yang, X. Tang, J. Wu, Z. Dong, Y. Yan, S. Zheng, J. Fan, X. Li, S. Cai and W. Zhang, *ACS Appl. Polym. Mater.*, 2022, **4**, 4624–4631.
42 D. Li, S. Zhang, J. Wan, W. Zhang, Y. Yan, X. Tang, S. Zheng, S. Cai and W. Zhang, *CrystEngComm*, 2021, **23**, 3594–3601.
43 W. Gong, Y. Dong, C. Liu, H. Shi, M. Yin, W. Li, Q. Song and C. Zhang, *Dyes Pigm.*, 2022, **204**, 110464.
44 J. Wan, W. Shi, Y. Li, Y. Yu, X. Wu, Z. Li, S. Y. Lee and K. H. Lee, *Macromol. Rapid Commun.*, 2022, **43**, 2200393.
45 S. Li, B. Zhao, W. Kan, T. Song, W. Zheng, X. Qi, L. Wang and B. Song, *Dyes Pigm.*, 2023, **214**, 111178.
46 A. Panda, Y. Yang, S. Venkateswarlu, Y. Son, T. Bae and M. Yoon, *Microporous Mesoporous Mater.*, 2020, **306**, 110399.
47 A. F. M. El-Mahdy, M. Lai and S. Kuo, *J. Mater. Chem. C*, 2020, **8**, 9520–9528.
48 J. Yang, Y. Cao, W. Si, J. Zhang, J. Wang, Y. Qu and W. Qin, *ChemSusChem*, 2022, **15**, e202200100.
49 P. Das, G. Chakraborty and S. K. Mandal, *ACS Appl. Mater. Interfaces*, 2020, **12**, 10224–10232.
50 Y. Cao, L. Zhang, J. Yang, J. Zhang, W. Si, J. Wang, A. Iqbal, W. Qin and Y. Liu, *Sens. Actuators, B*, 2021, **346**, 130472.
51 L. Liu, C. Wang, J. Wang, S. Jiang, W. Ma, Y. Zou and W. Tian, *J. Polym. Sci.*, 2023, **62**, 1609–1620.
52 J. Wang, C. Wang, S. Jiang, W. Ma, B. Xu, L. Liu and W. Tian, *J. Mater. Chem. C*, 2022, **10**, 2807–2813.
53 C. Liang, H. Lin, Q. Wang, E. Shi, S. Zhou, F. Zhang, F. Qu and G. Zhu, *J. Hazard. Mater.*, 2020, **381**, 120983.
54 S. Nandi, M. Sk and S. Biswas, *Dalton Trans.*, 2020, **49**, 12565–12573.
55 Y. Zhang, Y. Zhang, D. Zhang, S. Li, C. Jiang and Y. Su, *Sens. Actuators, B*, 2019, **285**, 607–616.